4 DOFs hollow soft pneumatic actuator – HOSE

Manfredi, Luigi; Putzu, Fabrizio; Guler, Saygun; Huan, Yu; Cuschieri, Alfred

Published in:
Materials Research Express

DOI:
10.1088/2053-1591/aaebea

Publication date:
2019

Document Version
Peer reviewed version

4 DOFs Hollow Soft Pneumatic Actuator - HOSE

Luigi Manfredi[1,*], Fabrizio Putzu[2], Saygun Guler[3], Yu Huan[4,5] and Alfred Cuschieri[1]

[1]Institute for Medical Science and Technology (IMSaT), University of Dundee, UK
[2]Queen Mary, Faculty of Science and Engineering, Queen Mary University of London, London, UK
[3]Faculty of Health and Social Sciences, Bournemouth University, Bournemouth, UK
[4]BioRobotics Institute, Scuola Superiore Sant'Anna, Pisa, Italy
[5]Center for Micro-BioRobotics, Istituto Italiano di Tecnologia (IIT), Pontedera, Italy

***Abstract*—This study reports a novel Hollow Soft Pneumatic Actuator (HOSE), which exhibits 4 degrees of freedom (DOFs). The design consists of a central hollow cylinder surrounded by four twisting symmetric chambers. By virtue of their spiral disposition, each chamber produces a diagonal force along the hollow internal cylinder composed of two components: one parallel to the Z axis and the other one to the plane X-Y. Both top and bottom sections of the actuator are reinforced to avoid deformation, essential for optimal function and dexterity of HOSE. Different movements of the actuator are produced by varying the activation combinations of the 4 chambers. They are constructed from thin walled (0.5 mm) Ecoflex 00-30 super soft silicon rubber, enabling HOSE to perform controlled movements with low pressure not exceeding 35 kPa.**

HOSE exhibits a maximal extension of 230% of its original length, bends up to i) $\pm 90^0$ around X axis, ii) $\pm 115^0$ around Y axis, and iii) twists around Z axis with a total range of $\pm 35^0$. The paper describes the manufacturing process together with the actuator performance, reporting the range of motion along each DOF related to the internal pressure, volume vs. forces and torques produced along each axis.

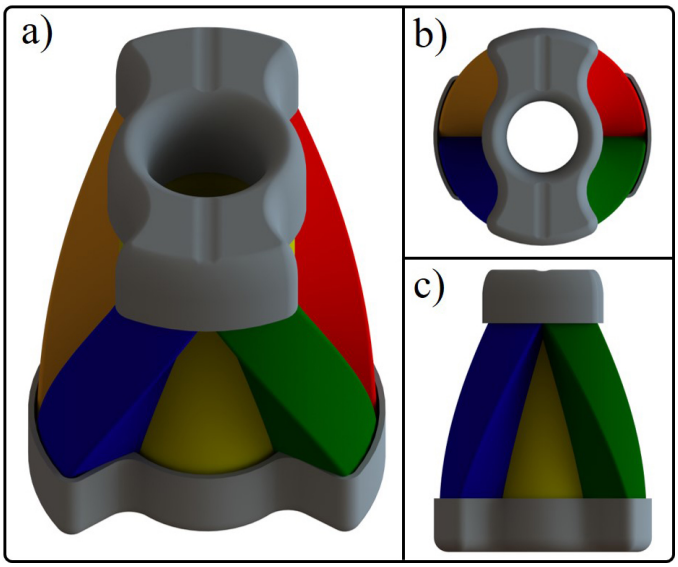

Fig. 1. a) HOSE 4 DOFs prototype, b) top view, and c) front view. Height h = 40 mm, diameter D = 30 mm, inner diameter ID = 10 mmm and a weight m = 9.4 g. It can rotate around 3 axes, and extend along one more axis.

I. INTRODUCTION

Over the last decade roboticists have tended to move away from designing rigid heavy robots to soft and lighter systems. The rigidity was a major requirement related to high precision and mechanical bandwidth, essential for precise industrial and surgical applications. The latter application imposed an additional requirement, i.e., safe interaction with human tissues and organs to avoid collateral damage. For this reason, researchers initially explored compliant robots based on the use of active sensing and control with rigid links, or by using intrinsically compliant materials [1]. In sharp contrast to rigid counterparts, soft robots are composed of continuously deformable soft structural components with high adaptation and response. Some soft robots are composed of materials with different stiffness [2]–[5].

The design of a soft robot with several degrees of freedom (DOFs) can be obtained by connecting several of these actuators to enhance its dexterity. This consideration led us to address a novel actuator design, which in essence, consists of a central hollow cylinder surrounded by 4 external soft pneumatic chambers. The resulting actuator (HOSE) is constructed from Ecoflex 00-30 with reinforced top and bottom sections. This novel design allows HOSE to bend in two directions, extend and rotate along one more axis, with a total of 4 DOFs. This provides the system with high dexterity, representing an improvement over the 3 DOFs previous systems [6]–[8]. The additional 4th DOF provided by HOSE is important since it enables the rotation essential to perform certain tasks. The additional requirements addressed by the design include: i) simple and low-cost manufacturing process, ii) inner hollow section for routing and instrument channels, iii) light weight, and iv) low actuating pressure. The manufacturing process is described and the performance in terms of range of motion, forces and torques produced by the actuator are reported.

A. Soft robotics: current state of the art

One of the first pneumatic actuators was reported by McKibben in the 1950's, who proposed a design which consisted of an inner rubber tube with a braided polyester mesh sleeve. The device could provide a pull-force akin to human muscles [9]. Connoly et al. proposed a fibre-reinforced soft actuator [10], exhibiting 1 DOF and capable of extension, bending, twisting, or contracting by varying the angle of the fibre. The behaviour

*Corresponding author: Luigi Manfredi, Institute for Medical Science and Technology (IMSaT), University of Dundee, Wilson House, 1 Wurzburg Loan, Dundee Medipark, Dundee DD2 1FD, UK, Phone: +44 (0) 1382 3881099, email: mail@luigimanfredi.com.

of the actuator was demonstrated in a simulator and validated by experimental characterization.

Suzumori et al. reported the first 3 DOFs pneumatic micro-actuator composed of 3 chambers, with an external diameter of 12 mm and a total length of 120 mm [6]. The actuator was made from fibre reinforced rubber and actuated by an electro-pneumatic or electro-hydraulic system. Performance of the device was variously reported as a single actuator, as a micro manipulator and as a small walking quadruped.

Marchese et al. reported a soft arm capable of uni-planar movement composed of 4 modules [11]. Subsequently they improved the system with the development of a soft spatial arm also with 4 modules, each exhibiting 2 DOFs [12]. This was composed of 4 chambers made of Ecoflex and an inner layer made of a stiffer soft material. The air volume in each chamber was controlled by using a linear actuator moving a piston inside a fluid cylinder.

Other reports have described pneumatic systems for bendable actuators with use of 3 straight chambers providing a total of 3 DOFs [7], [8]. Each chamber could produce a pushing force, in order to bend the actuator in one direction. The combined simultaneous activation of the chambers resulted in 2 DOFs bending and 1 DOF for extension of the actuator, providing a total of 3 DOFs.

Marchese et al. reported a detailed description for the design and fabrication of soft actuators by different techniques [13]. The importance of this report relates to the useful practical description of the moulding process and choice of the materials for different actuators and their performance.

The design of HOSE is described and illustrated in detail in section II and III, respectively.

II. Materials and Methods

A. Design

HOSE is a hollow soft pneumatic actuator with an external diameter D = 30 mm, an overall height h = 40 mm, internal diameter ID = 10 mm, and a total weight of 9.4 grams. As shown in figures 1 and 2, rectangular actuating pneumatic chambers spiral round a central circular cylinder. As distinct from previous reports of soft modules [7], [8], [11], [12] where chambers are straight, in the proposed design, when an outer spiral rectangular chamber i is inflated, it produces a force applied directly to the central passive hollow cylinder is produced. This force can be decoupled in two components: a minor and non dominant (ND) force (F'''_{Ci}), which is the force acting on the X-Y plane; one major dominant force perpendicular to the ND force and acting along Z axis (F_{Ciz}), as shown in figure 2.

All the ND forces play an important role in the dexterity of the actuator, as described in detail in section II-B. This design allows the combined activation of two chambers (Cs) to cancel part the F'''_{Ci} when these forces originate from chambers on the same side. The opposite result is obtained when the forces are generated from chambers lying diagonally opposite each other. They double the force acting on the central passive chamber, resulting in a twisting motion around the Z axis in either a positive (C_1-C_3) or negative direction (C_2-C_4).

When chambers from the same side are activated (C_1-C_2, C_3-C_4, C_1-C_4, C_2-C_3), part of the F'''_{Ci} force components acts in opposite directions and are thus absorbed by the structure of the actuator. The combination of chambers activations produces a rotation around the X axis (C_1-C_2 positive, C_3-C_4 negative as shown in figure 2-a)), or around the Y axis (C_2-C_3 positive, C_1-C_4 negative as shown in figure 2-b)).

When diagonally placed chambers are activated (C_1-C_3, C_2-C_4), the F'''_{Ci} force components are in an opposite direction and thus exert forces with different focal points, thereby producing a torque on the central hollow cylinder as shown in figure 2-c). Collapse of the inner hollow cylinder is prevented by reinforcement of its top and bottom sections. This is essential to enable rotation without squeezing the internal hollow central cylinder.

The angle between the chambers and the vertical Z axis defined as α_i (figure 2-a) and 2-b)) changes during the extension of the chamber resulting in a different behaviour of the actuator during its movement, as explained in section II.

The dexterity of HOSE is a trade-off between the overall diameter and height. The performance in terms of range of motion and output torque along each axis is defined by a constant parameter ϕ, which represents the ratio between the height (h) and the diameter (D), ($\phi = h/d$) of HOSE. When this value is greater than 1, the angle α_i closely approximates to 0° reducing the F'''_{Ci} forces and hence, the range of twisting motion. In this case, the chambers behave like straight chambers and the twisting effect is negligible. When $\phi \sim 1$, the F_{iz} components force along the Z axis is similar to the F'_{Ci} component in the X-Y plane. When $\phi < 1$, the F'''_{Ci} component starts to increase more than the F_{iz} force along the Z axis, increasing the twisting torque, but with reduction of the torque around X and Y axis resulting in a decrease in the overall extension. After several trials and different preliminary experiments, a design with $\phi = 4/3$ has been selected to obtain a compromise between the rotation ranges around each axis and the overall extension.

B. Statics

Figure 2 shows the forces of the chambers along X and Y axes. Part of the forces and torques produced by the 4 chambers are partially absorbed in the actuator structure. The resistance forces and torques produced by the actuator structure are related to the thickness of the walls and the Young's modulus of the elastomer. A thinner wall decreases this resistance although it can also reduce the reliability and the fatigue duration of the actuator. Each chamber i produces a force (F_{Ci}) which is related to its cross section area (A_i) and the air activation pressure (P_i), $F_{Ci} = A_i P_i$. The forces and torques produced by the structure (F_P, M_P) and the chambers (F_{Ci}, M_{Ci}) of the actuator are following described:

$$\begin{aligned} F_P &= (-F_{Px}, -F_{Py}, -F_{Pz}) \\ M_P &= (-M_{Px}, -M_{Py}, -M_{Pz}) \end{aligned} \tag{1}$$

$$\begin{aligned} F_{Ci} &= (F_{Cix}, F_{Ciy}, F_{Ciz}) \\ M_{Ci} &= (M_{Cix}, M_{Ciy}, M_{Ciz}) \end{aligned} \tag{2}$$

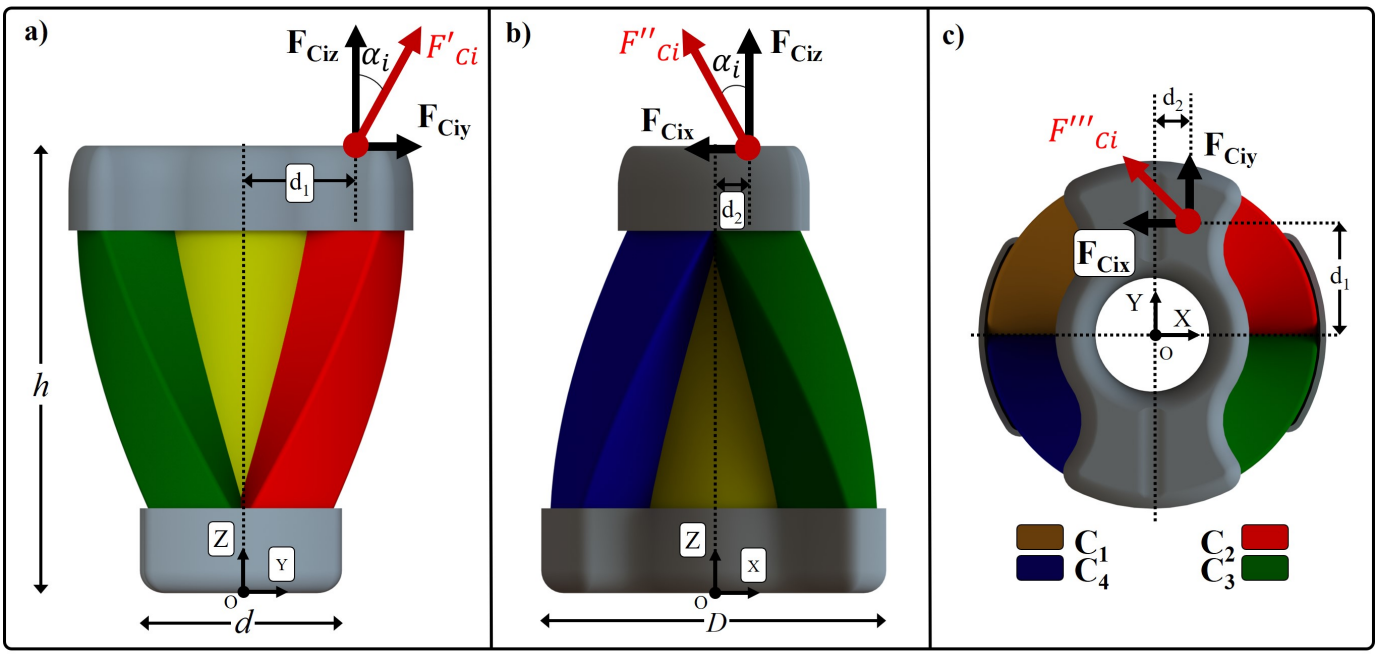

Fig. 2. Figure a) shows the front view of the actuator with the resultant of the force of the chamber i projected in the plane Y-Z, F'_{Ci}, applied to the top of the actuator at a distance d_1. Figure b) shows the front view of the actuator with the resultant of the forces of the chamber i projected in the plane X-Z, F''_{Ci}, applied to the top of the actuator at a distance d_2. Figure c) shows the top view of the actuator with the resultant of the forces of the chamber i projected in the plane X-Y, F'''_{Ci}, applied to the top of the actuator at a distance $\sqrt{{d_1}^2 + {d_2}^2}$.

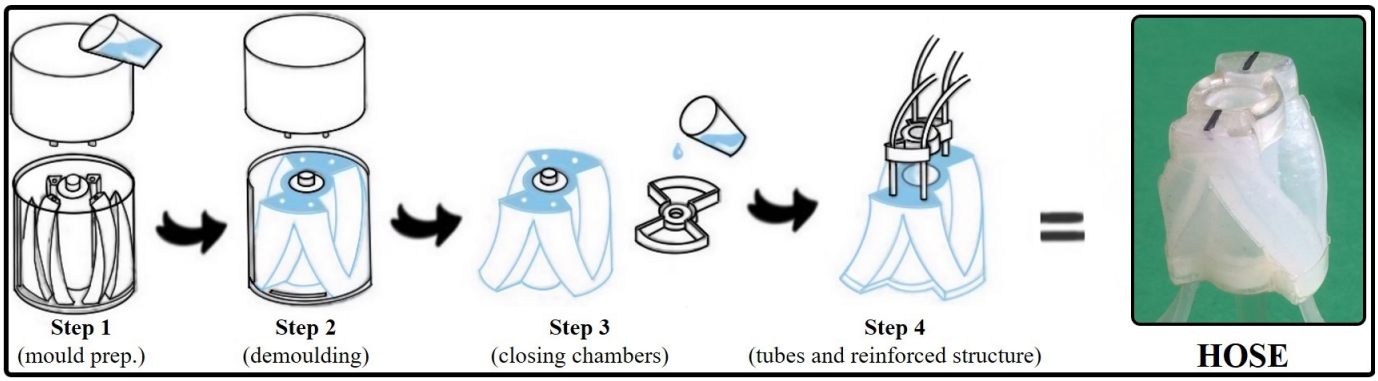

Fig. 3. Production sequence of HOSE in 4 steps: *Step-1* assembly of the mould; *Step-2* silicon poured in mould and in *Step-3* demoulding with closure of bottom of chambers; *Step-4* reinforcement of the top and bottom sections. On the right, the final version of HOSE with tubes inserted, and reinforced top and bottom sections is shown.

The force components along the X and Y axes are:

$$\begin{aligned} F_{Cix} &= F''_{Ci} sin(\alpha_i) \\ F_{Ciy} &= F'_{Ci} sin(\alpha_i) \\ F_{Ciz} &= F'_{Ci} cos(\alpha_i) = F''_{Ci} cos(\alpha_i) \end{aligned} \tag{3}$$

The statics of the system is described by the following equations:

$$\begin{aligned} \sum F_{ix} = \sum F_{iy} = \sum F_{iz} = 0 \\ \sum M_{ix} = \sum M_{iy} = \sum M_{iz} = 0 \end{aligned} \tag{4}$$

and considering the equations 1 and 2, the equation 4 becomes as follows:

$$\sum F_{i_X} = (F_{C1x} + F_{C4x}) - (F_{C2x} + F_{C3x}) - F_{Px} = 0 \tag{5}$$

$$\sum F_{i_Y} = (F_{C1y} + F_{C2y}) - (F_{C3y} + F_{C4y}) - F_{Py} = 0 \tag{6}$$

$$\sum F_{i_Z} = (F_{C1z} + F_{C2z} + F_{C3z} + F_{C4z}) - F_{Pz} = 0 \tag{7}$$

$$\begin{aligned} \sum M_{i_X} = [(F_{C1z} + F_{C2z})d_1 - (F_{C1y} + F_{C2y})h] + \\ - [(F_{C3z} + F_{C4z})d_1 - (F_{C3y} + F_{C4y})h] + \\ - M_{Px} = 0 \end{aligned} \tag{8}$$

$$\begin{aligned} \sum M_{i_Y} = [(F_{C1z} + F_{C4z})d_2 + (F_{C1x} + F_{C4x})h] + \\ - [(F_{C2z} + F_{TC3z})d_2 + (F_{C2x} + F_{TC3x})h] + \\ - M_{Py} = 0 \end{aligned} \tag{9}$$

$$\begin{aligned} \sum M_{i_Z} = [(F_{C2y} + F_{C4y})d_2 + (F_{C2x} + F_{C4x})d_1] + \\ - [(F_{C1y} + F_{C3y})d_2 + (F_{C1x} + F_{C3x})d_1] + \\ - M_{Pz} = 0 \end{aligned} \tag{10}$$

where $h > d_1 > d_2$.
As described by the equation 2, the activation of a chamber produces a force and a torque with components along the 3 axes. The equation 7 shows that the resultant of the force along the Z axis cannot be cancelled with any combined chamber activation. This force causes an extension of HOSE along Z axis when any chamber is activated. This implies that a rotation around each axis (X, Y, Z) is combined with an extension of the actuator along the Z axis. This behaviour is experimentally reported in section IV.

C. Trade-off between straight and spiral chambers

Activation of a spiral chamber in HOSE causes a ND component force which twists the actuator around its Z axis. Bending of HOSE around both X and Y axes is induced by partial absorption by its structure with consequential dissipation of the applied energy during its motion and hence reduced actuator energy efficiency.

In soft actuators consisting of only straight chambers, the forces produced are aligned along the Z axis resulting in a force along the rotational axis. Hence, in a actuator with 4 straight chambers and 2 DOFs [13], movement around X axis or Y axis is produced by the activation of only one chamber. In contrast, in a soft actuator with 3 straight chambers and 3 DOFs [6], [7], activation along one axis is obtained by the activation of one or more chambers, with consequential reduced energy efficiency. In both actuators, the rotation along an arbitrary axis in the X-Y plane requires a combined activation of more than one chamber.

Extension along Z axis is produced by a combined activation of all the chambers with higher efficiency. The partial energy absorption by the 4 spiral chambers of HOSE accounts for its extension along the Z axis. This implies that systems with parallel chambers are more efficient than HOSE. The HOSE ϕ parameter is related to its performance and also to its energy efficiency, i.e., the higher the ϕ, the higher the energy efficiency.

D. Manufacturing

HOSE is constructed from Ecoflex 00-30 in view of its excellent properties (shore hardness = 00-30, tensile strength= 1,38 MPa, 100% modulus = 68,95 kPa, elongation at break of 900%) using the following manufacturing process, described in 4 steps (figure 3) and with use of a 3D printed mould (figure 4).

Step-1: Ecoflex 00-30 parts A and B are mixed in a 1:1 ratio and then vacuumed at 0 atm for 10 minutes to remove air, to prevent bubble formation in the cast. The Ecoflex mixture is then poured into the mould (figure 4-d)) and left to cure either at room temperature for 4 hours or by speeding the curing process by heating in an oven at 60° Celsius for 30 minutes. After curing, the external (M_8, M_9), bottom and top (M_{12}, M_{13}), and lateral (M_6, M_7, M_{10}, M_{11}) parts of the mould are removed.

Step-2: the extensions of the mould inside the chambers are then removed (M_2, M_3, M_4, M_5) leaving them hollow while keeping the mould extension inside the inner cylinder (M_1). This process ensures the central cylinder remains stiff and facilitate its manipulation during the subsequent stage.

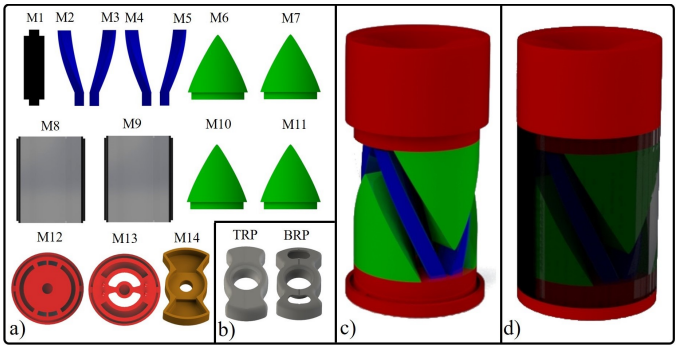

Fig. 4. Mould used to construct HOSE: a) composed of 14 parts; b) reinforced 3D printed parts (TRS, BRS) to increase the stiffness and the range of motion, with BRP having two open sections for connection of silicon tubes to the chambers; c) and d) show the mould without the external transparent walls (M_8-M_9) and with all the components. The lateral walls (M_8 and M_9) are printed with transparent material to enable inspection for air bubble formation during the pouring of Ecoflex into the mould.

Step-3: an additional mould (M_{14}) is used to construct the bottom section of HOSE needed to close the base of the chambers, also with Ecoflex 00-30.

Step-4: during this step, four silicon tubes with an external diameter of 2.1 mm are glued to the upper holes of the actuator with Loctite® superglue. The top and bottom reinforced parts (TRS and BRS, figure 4-b), which have an external diameter of 30 mm and a wall thickness of 0.5 mm, are essential for reinforcement of the structure, to prevent deformation and to increase the twisting around the Z axis during inflation. They are 3D printed from VeroClear-RGB10 polymer. Both TRS and BRS are glued to the soft Ecoflex with Loctite® superglue. The prototype produced by this process is shown in figure 3.

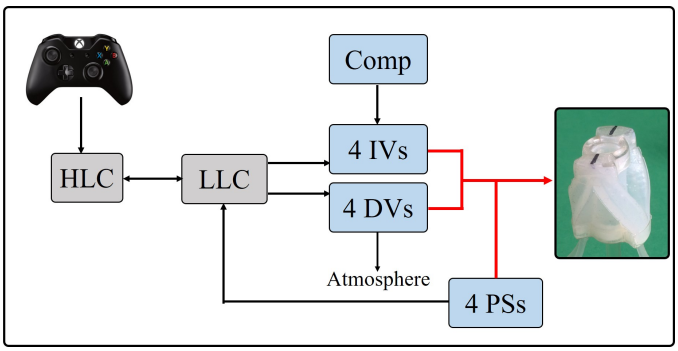

Fig. 5. Control hardware architecture consisting of an Xbox One wireless controller, a PC with high-level control (HLC), an Arduino board for the low-level control (LLC), 8 electro valves (EV_s), 4 pressure sensors (PS_s), and an external compressor. The black lines represent electrical wires and the red lines air tubes.

III. Control Hardware

A preliminary and simple open-loop control hardware was designed using off-the-shelf components to evaluate the manoeuvrability of HOSE (figure 5). A total of 8 electro-valves (EVs), 4 to inflate and 4 others to deflate, are used to control

the air volume and pressure inside the 4 chambers. An external compressor provides the air for inflation of the chambers.
With the inflow valve (IV) closed (prior to activation of the chamber), the pressure within the chamber equals atmospheric pressure. When the IV is opened for air insufflation by the compressor and the outflow valve (OV) is closed, the pressure rises and the chamber is activated. When both the IV and OV are closed, the air volume inside the chamber is fixed. When the OV is opened and the IV is closed, the pressure in the chamber drops to reach atmospheric. Each chamber has an analogue pressure sensor (PS) used to monitor its intraluminal pressure and to limit the maximal pressure applied to each chamber to prevent damage.
Both valves and sensors are connected to an Arduino board, which works as a bridge interface (BI) and implements a low-level control (LLC), the role of which is to activate/deactivate the EVs and to acquire the 4 analogue PSs. The role of the BI is for data exchange with the external interface (EI) through a serial communication port.
The high-level control (HLC) is implemented in Matlab® Simulink and includes a serial communication interface to the LLC and the Xbox One wireless controller. The control architecture is designed to perform simple movements of the actuator by using an open-loop on-off control and visual feedback by the operator.

IV. Results and discussions

The performance of HOSE was evaluated by measuring the pressure, volume, and range of motion for each DOF. In addition, the forces and torques generated were measured by a dedicated force torque sensor. Each actuation test for every DOF was performed 3 times with incremental increase of the air volume at each step. The mean value and standard deviation are plotted in the graphs. Each chamber received a total volume of 100 mL delivered by 4 air pistons in incremental air volume of 5 mL, at each step. The activation configuration is reported in table I and the performance in table II.

TABLE I
Chambers activations

Axes Range	Chambers activation
+X (Rotation)	C_1-C_2
-X (Rotation)	C_3-C_4
+Y (Rotation)	C_1-C_4
-Y (Rotation)	C_2-C_3
+Z (Rotation)	C_2-C_4
-Z (Rotation)	C_1-C_3
Z (Extension)	C_1-C_2-C_3-C_4

A. Bending: rotation around X and Y axes

HOSE can bend around both X and Y axes, by ipsilateral activation of chambers, with the central hollow cylinder acting as a fulcrum. The forces generated by the chambers activation are shown in figure 2-a) and 2-b), respectively.
When two consecutive chambers are activated, the rotation around X axis behaves differently from the rotation around Y axis. Both rotations produce a force and torque reaction from the central hollow cylinder, this being responsible for bending and extension of HOSE. The ND force components (F'''_{Ci}) along the X or Y axes are equal but in the opposite direction. Hence, they are absorbed by the structure of HOSE. The other components along Y or X axes are equal and in the same direction, hence producing the rotation of HOSE. When the actuator extends, α_i decreases, hence the F'''_{Ci} forces decrease.
In the rotation around Y axes the central cylinder is subjected to a force applied at a distance d_2, which is lower than d_1 in the X rotation. The ND forces in the rotation around the Y axes have an opposite direction to the ones around the X axes. This results in an increased bending of the central cylinder around Y axis compared to the bending around X axis. Figure 6 shows the actuator bending around X and Y axes. The rotation around each axis is combined with and extension along Z axis. When the rotation is around X axis, the opposite directions of the ND components produce an extension of the actuator higher than the one produced in the rotation around Y axis.
The graphs relating pressure vs. volume encompass 4 phases: i) activation, ii) motion - decreasing pressure, iii) motion - increasing pressure, and iv) saturation. The activation phase shows discontinuous pressure resulting in a negligible movement of the tip of HOSE, which is considered as the activation pressure and minimum inflation volume, i.e., the minimum value required to induce movement in HOSE. Phase ii) defined as when HOSE starts to bend, results in a reduction of the pressure as the bending increases. There are three reasons to explain this. The first is the change in angle α_i when the actuator bends, with consequent reduction of the ND components, effectively resulting in all the forces produced by HOSE being in line with Z axis. In turn, this increases the torque applied to the tip of HOSE and therefore induces bending. The second reason is that the central hollow cylinder as it bends, becomes floppy with reduced pressure inside the chambers. The third reason is the increased wall tension when the diameter of the chambers increases (Laplace's law) in relation to the mechanical properties of Ecoflex. In phase iii) the pressure increases again till phase iv). In phase iv), when HOSE is saturated, there is a rising pressure with a negligible effect on bending, which eventually induces a wall tension close to the bursting point of the chamber.
The graphs relating volume vs. range of motion show similar profiles around X and Y axes. They are monotonic with an activation volume of circa 20 mL and a saturation phase of motion when a volume of 200 mL is inflated in both activated chambers.

B. Twisting: rotation around Z axis

HOSE twists and extends on activation of diagonally opposite chambers (figure 7).
The activation of the diagonally opposite chambers produces a diagonal force composed of dominant components ($F'_{Ci}+F''_{Ci}$) along Z axis, and a smaller ND component (F'''_{Ci}) in the X-Y plane. The F'''_{Ci} has two components: one is compensated by the activation of the other, with the second being involved in the twisting of HOSE (figure 2-c)).
The ND components involved in the rotation are opposite

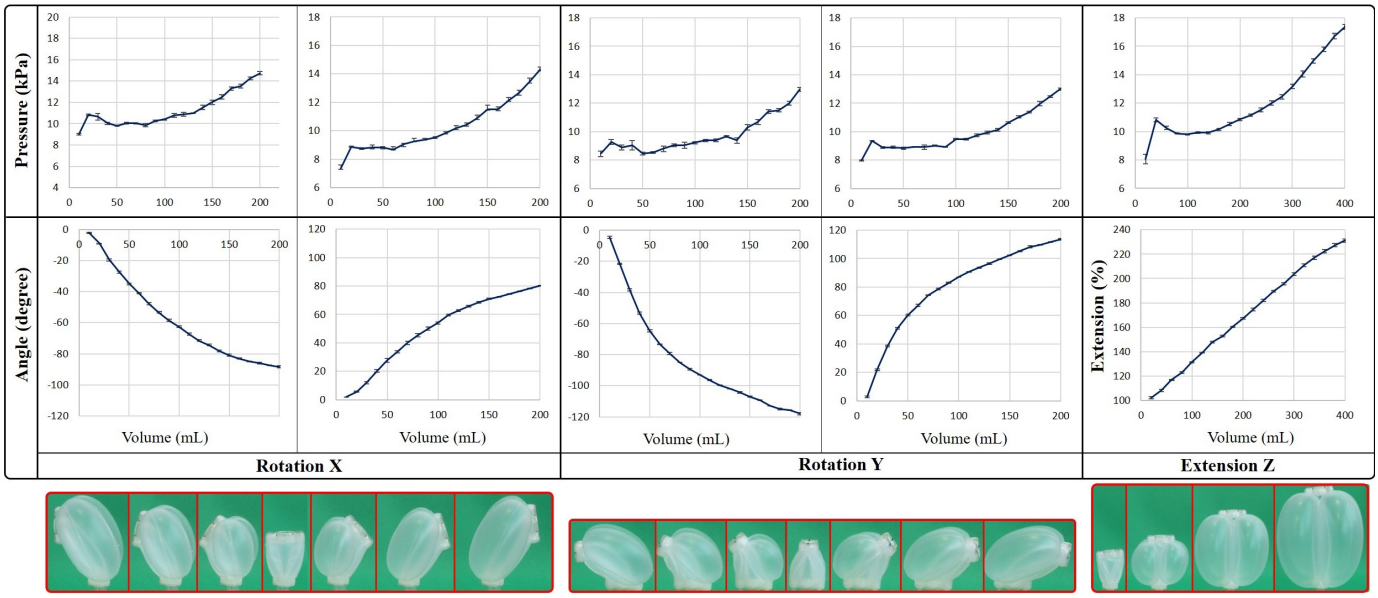

Fig. 6. Volume vs. pressure, and volume vs. range of motion graphs during activation around X and Y axes and extension along Z axis. The error bars show the standard deviation from the mean value obtained by performing the experiments in triplicate for each experiment.

in direction and applied at a distance of $2d_1$, producing a torque around the central hollow cylinder, causing the rotation of the actuator in two directions. The F'''_{Ci} (in the X-Y plane) is higher during the activation (when α_i is higher), and decreases as HOSE extends, reaching saturation of the twisting angle around Z axis. Figure 7 outlines the twisting performance.
The activation of the diagonally opposite chambers produces twisting with simultaneous extension of HOSE. This effect is related to the design parameter ϕ. The graphs in figure 7 shows the relation between twisting and extension by defining 2 parameters, λ and η.

$\lambda = \delta/\delta_M$ represents the percent twisting angle to the total twisting range of motion. It is evident that 90% of the total range is achieved when just over half (110 mL) of the total 200 mL of air is inflated.

$\eta = \delta/\rho$ represents the ratio between the percent range of twisting vs. the percent extension. This graph (figure 7) illustrates that in the initial phase (0 to 70 mL) the value increases, and then decreases mainly due to extension rather than twisting.

On considering both parameters, it is evident that when a volume from 0 to 70 mL is inflated the twisting predominates over extension. Thereafter (70 to 110 mL) extension starts to dominate over twisting, until beyond 110 mL, when twisting is negligible and extension becomes dominant.

C. Extension

The extension of HOSE is achieved by simultaneous activation of all the chambers as shown in figure 6. Radial expansion occurs to the same extent.
Figure 6 shows the extension performance of the actuator. After the activation phase, the air volume increases although the pressure decreases. The extension vs. volume profile is almost linear.

D. Volume and Pressure profile

Positive and negative values of the range of motion are shown in all graphs during both bending and twisting experiments although they are not perfectly symmetric (figures 6 and 7). This effect is due to the non-asymmetric distribution of wall thickness in all the chambers, caused by the moulding process.
All the reported volume vs. pressure graphs show a pressure that decreases after the first activation phase, ranging from 0 to circa 10 mL of air for each chamber in phase ii), and then increases in phase iii). This implies that the pressure is not a suitable variable for the implementation of a closed-loop control system. Pressure sensors must be used as a safety control to monitor the stress of the material.
The air volume profile in the range of motion and during all the experiments is described by a monotonic function which makes this variable suitable for a closed-loop control. The volume vs. range of motion graphs have an almost linear profile during the extension.

E. Force and Torque profile

HOSE was tested by measuring the output torques and forces along each axis. The experiments were performed by using a 3D force and 3D torque sensor connected to a set-up shown in figure 9 . Each experiment was performed three times in a quasi-static configuration with the actuator in the rest position and inflating 5 mL of air in each chamber for an overall volume of 100 mL in each chamber. The forces and torques were measured by inflating two and four chambers together, with measurement of the total volume and total pressure in all the chambers.

Force

During rotations around X, Y and Z axes, and extension along Z axis, the dominant force exhibits two linear phases

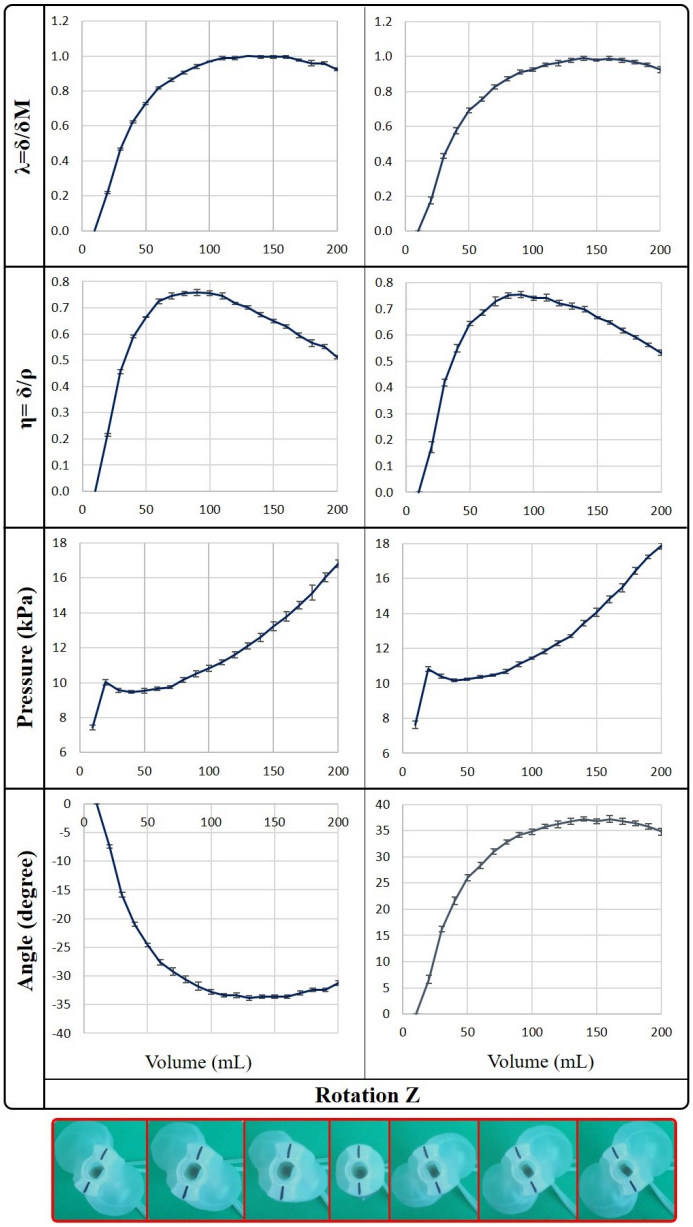

Fig. 7. Volume vs. pressure, and volume vs. range of motion graphs in the rotation around Z axis. In the twist activation $\lambda = \delta/\delta_M$ represents the percentage of twisting angle to the total range of motion. $\eta = \delta/\rho$ defines the ratio between the percentage of twisting range vs. the percent of extension.

after the activation phase. The first one ranges from 0 to circa 60 mL volume of air in each chamber. In this phase, the pressure after the initial step remains almost constant, rendering the increase of the volume the only variable causing the output force. The second phase has a higher slope from 60 mL to 100 mL. During this phase, the pressure and volume start to increase, resulting in an incremental increase of the output force, reflected by a higher slope. In all the graphs, the force along Z axis is higher than the other components along X and Y axis. The maximal force and force to weight ratio achieved by HOSE are shown in Tab. II.

Torque

The torque around X axis is much higher than the one around Y axis. This is explained by the statics of the actuator as described in section II-B and as shown in figure 2. The torque around Z is also higher than the torque along Y but lower than the torque around X. The expansion of each chamber affects the distance of the applied force resulting in a higher torque as the air volume increases. The maximal torque and torque to weight ratio achieved by HOSE are shown in Tab II.

TABLE II
MODULE PERFORMANCES

X Rotation	(+80.3°,-88.3°) @ (13.0, 13.0) kPa
Y Rotation	(+113.7°,-118.0°) @ (13.0, 13.0) kPa
Z Rotation	(+34.8°,-31.2°) @ (17.9, 16.8) kPa
Z Extension	231.2% @ 17.3 kPa
X Torque	(+114.2, -111.8) Nmm @ (17.2, 16.5) kPa
Y Torque	(+34.9, -32.7) Nmm @ (19.4, 19.5) kPa
Z Torque	(+41.8, -43.8) Nmm @ (17.8, 18.9) kPa
Z Force	15.9 N @ 15.5 kPa
Force to weight ratio	1.69 N/g
Torque to weight ratio	19.18 Nmm/g

V. CONCLUSIONS

A design of a Hollow Soft Pneumatic Actuator (HOSE) with 4 DOFs is presented, including the description of the manufacturing process and the performance of the soft actuator in terms of range of motion. The forces and torques produced along each axis are reported in table II.

The novelty in this design is the combination of 4 DOFs in one actuator by using only 4 chambers. HOSE exhibits good dexterity along each DOF with a low input pressure and a maximal output force of 16 N, and a torque of 114 Nmm over a weight of only 9.4 grams, a force to weight ratio up to 1.69 N/g, and a torque to weight ratio up to 19.18 Nmm/g. The hollow central cylinder can be used for routing the actuation tubes and electrical cables and to embed any electronic board on the top part of the actuator for execution of more complex tasks, such as camera holder, spherical wrist, etc.

The range of rotation around each axis is related to: the overall length of the actuator; the spiral shape of the chamber; the wall thickness; the ϕ parameter, which represents the ratio between the height and the diameter of HOSE.

The hardware control of HOSE was configured from off-the-shelf components and the overall architecture is simple to produce. A preliminary on-off control system has been implemented to perform simple movements by using an Xbox One wireless controller. Improvements are necessary, including implementation of a closed-loop control by additional sensors to detect the position and orientation of the top part of the actuator.

Future R&D will be directed towards the improvement of the electronics and small valves embedded. Ultimately, the authors intend to design and produce a modular module capable of translating complex manipulation based on several HOSE units.

The combined rotation and extension can limit the application of HOSE when a rotation around a fixed point is required.

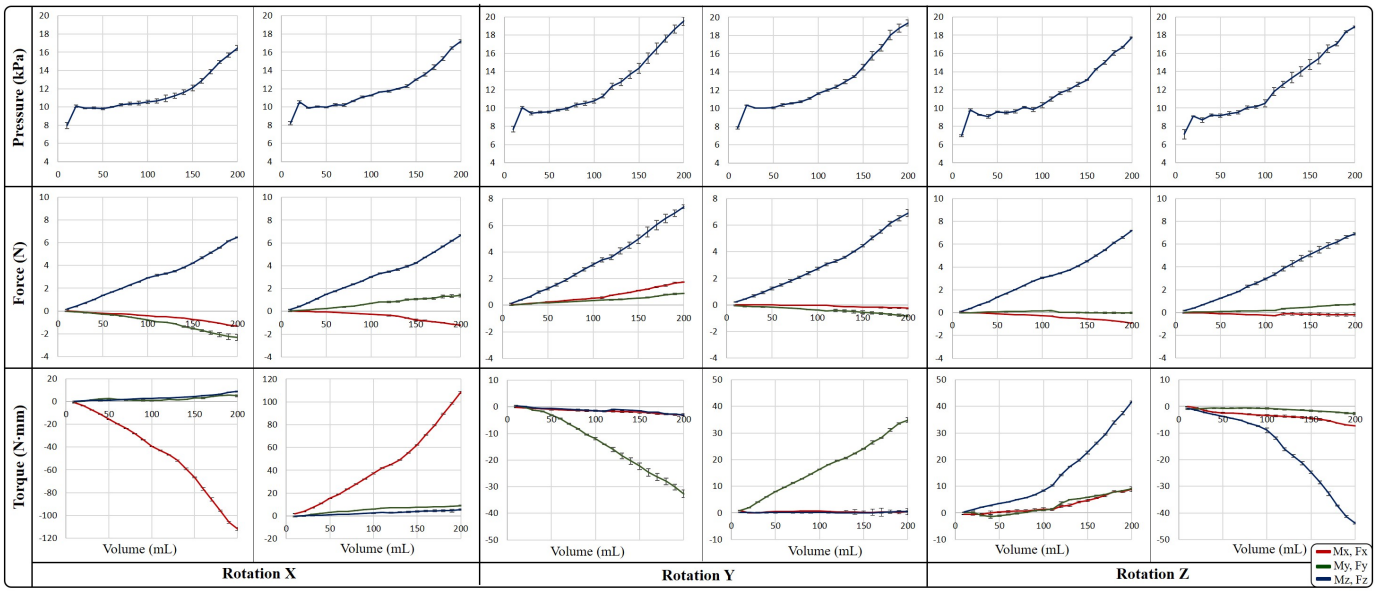

Fig. 8. Pressure vs. volume and 3D Forces and 3D torque vs. volume profile with HOSE in the rest position when performed rotation around X-axis, Y-axis and Z-axis. The volume and pressure reported in the graphs, are the total applied to all the chambers.

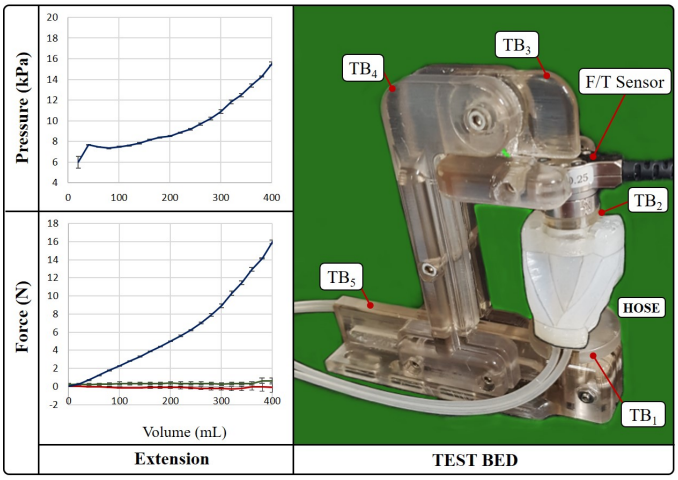

Fig. 9. Pressure vs. volume and 3D Forces and 3D torque vs. volume profile with HOSE in the rest position. The volume reported in the graphs are the total applied to all the chambers, and the pressure the average value of the all the chambers.
All the reported experiments were performed by using a test bed (TB) with an adjustable set up composed of 5 parts. HOSE is fixed to the TB by TB_1 and to the F/T sensor by TB_2. The F/T sensor is connected to the TB by TB_3, which is connected to the TB_4 by means of a fulcrum, allowing a rotation around it. TB_4 is connected to the TB5 by two screws allowing a horizontal movement. TB_3 can have different lengths to allow lateral expansion of the joint.

In this case, at least one more actuator connected to the base of HOSE is needed to compensate for the extension. This increases the complexity of the kinematic control. There is also a need to explore reinforced silicon structure to minimize the balloon effect and to reduce material fatigue thereby preserving or prolonging the high dexterity achieved by this novel design.

Other studies will investigate on an analytic model of the actuator to define the optimal configuration in terms of chamber length, orientation and size, to increase the range of motion, and reduce the maximal pressure.

The simple manufacturing process has several advantages including miniaturization of this soft actuator for use in several biomedical applications in which the operative work space is confined. The dexterity of the actuator will certainly be advantageous for applications requiring manipulation of an end effector or camera manoeuvres for inspection.

Author Disclosure Statement

No competing financial interests exist.

References

[1] B. Vanderborght, A. Albu-Schaeffer, A. Bicchi, E. Burdet, D. Caldwell, R. Carloni, M. Catalano, O. Eiberger, W. Friedl, G. Ganesh, M. Garabini, M. Grebenstein, G. Grioli, S. Haddadin, H. Hoppner, A. Jafari, M. Laffranchi, D. Lefeber, F. Petit, S. Stramigioli, N. Tsagarakis, M. V. Damme, R. V. Ham, L. Visser, and S. Wolf, "Variable impedance actuators: A review," *Robotics and Autonomous Systems*, vol. 61, no. 12, pp. 1601 – 1614, 2013. [Online]. Available: http://www.sciencedirect.com/science/article/pii/S0921889013001188

[2] G. Sumbre, G. Fiorito, T. Flash, and B. Hochner, "Octopuses use a human-like strategy to control precise point-to-point arm movements," *Current Biology*, vol. 16, no. 8, pp. 767 – 772, 2006. [Online]. Available: http://www.sciencedirect.com/science/article/pii/S0960982206012747

[3] L. Margheri, C. Laschi, and B. Mazzolai, "Soft robotic arm inspired by the octopus: I. from biological functions to artificial requirements," *Bioinspiration & Biomimetics*, vol. 7, no. 2, p. 025004, 2012. [Online]. Available: http://stacks.iop.org/1748-3190/7/i=2/a=025004

[4] C. Laschi, B. Mazzolai, and M. Cianchetti, "Soft robotics: Technologies and systems pushing the boundaries of robot abilities," *Science Robotics*, vol. 1, no. 1, 2016. [Online]. Available: http://robotics.sciencemag.org/content/1/1/eaah3690

[5] F. Maghooa, A. Stilli, Y. Noh, K. Althoefer, and H. A. Wurdemann, "Tendon and pressure actuation for a bio-inspired manipulator based on an antagonistic principle," in *2015 IEEE International Conference on Robotics and Automation (ICRA)*, May 2015, pp. 2556–2561.

[6] K. Suzumori, S. Iikura, and H. Tanaka, "Flexible microactuator for miniature robots," in *Micro Electro Mechanical Systems, 1991, MEMS '91, Proceedings. An Investigation of Micro Structures, Sensors, Actuators, Machines and Robots. IEEE*, Jan 1991, pp. 204–209.

[7] T. Ranzani, G. Gerboni, M. Cianchetti, and A. Menciassi, "A bioinspired soft manipulator for minimally invasive surgery," *Bioinspiration & Biomimetics*, vol. 10, no. 3, p. 035008, 2015. [Online]. Available: http://stacks.iop.org/1748-3190/10/i=3/a=035008

[8] A. D. Greef, P. Lambert, and A. Delchambre, "Towards flexible medical instruments: Review of flexible fluidic actuators," *Precision Engineering*, vol. 33, no. 4, pp. 311 – 321, 2009. [Online]. Available: http://www.sciencedirect.com/science/article/pii/S0141635908001190

[9] B. Tondu, "Modelling of the mckibben artificial muscle: A review," *Journal of Intelligent Material Systems and Structures*, vol. 23, no. 3, pp. 225–253, 2012. [Online]. Available: http://jim.sagepub.com/content/23/3/225.abstract

[10] F. Connolly, P. Polygerinos, C. J. Walsh, and K. Bertoldi, "Mechanical programming of soft actuators by varying fiber angle," *Soft Robotics*, vol. 2, pp. 26–32, 2015.

[11] A. D. Marchese, R. K. Katzschmann, and D. Rus, "Whole arm planning for a soft and highly compliant 2d robotic manipulator," in *2014 IEEE/RSJ International Conference on Intelligent Robots and Systems*, Sept 2014, pp. 554–560.

[12] A. D. Marchese and D. Rus, "Design, kinematics, and control of a soft spatial fluidic elastomer manipulator," *The International Journal of Robotics Research*, vol. 35, no. 7, pp. 840–869, 2016. [Online]. Available: https://doi.org/10.1177/0278364915587925

[13] R. K. K. Andrew D. Marchese and D. Rus, "A recipe for soft fluidic elastomer robots," *Soft Robotics*, vol. 1, no. 2, pp. 7 – 25, 2015. [Online]. Available: http://online.liebertpub.com/doi/abs/10.1089/soro.2014.0022